# Directional Stiffness-Switching Soft Robots via Phase-Changing Metallic Spines

Daniel S. Esser[1], *Student Member, IEEE*, Emily McCabe[1], *Student Member, IEEE*, Tayfun Efe Ertop[1], *Member, IEEE*, Alan Kuntz[2], *Member, IEEE*, and Robert J. Webster III[1], *Senior Member, IEEE*

***Abstract*— Conventional soft robots are designed with constant, passive stiffness properties, based on desired motion capabilities. The ability to encode two fundamentally different stiffness characteristics promises to enable a single robot to be optimized for multiple divergent tasks simultaneously and this has been previously proposed with a variety of approaches including jamming-based designs. In this paper, we propose phase-changing metallic spines of various geometries to independently control specific directional stiffness parameters of soft robots, changing how they respond to their actuation inputs and external loads. We fabricate spine-like structures using a low melting point alloy (LMPA), enabling us to switch on and off the effects of the stiff metal structure of the overall robot's stiffness during use. Changing soft robot morphology in this manner will enable these robots to adapt to environments and tasks that require divergent motion and force/moment application capabilities.**

## I. INTRODUCTION

Soft robots are typically optimized for a single kind of task. For example, high flexibility is desired in constrained environments to ensure safety in the event of unanticipated robot-environment collisions. Conversely, stiffness is desired when the robot must manipulate heavy payloads. This trade-off is fundamental; compliance is desired for safety and stiffness for applying forces. Typically these conflicting objectives require the designer to choose robot parameters that are non-optimal for both objectives individually.

Towards obtaining the best of both, researchers have sought variable stiffness designs for continuum robots. These include multi-backbone robots with mechanically actuated secondary backbones that change stiffness along part of the robot for fine motion control [1] or to shift the workspace [2]. Another approach is to use antagonistic tendon actuation to modify stiffness [3]. Pneumatic bellows have also been combined with tendons to enable antagonistic stiffening [4]. Magnetic mechanisms have been proposed to lock a segment of a tendon-actuated robot into a curved shape while using the same tendon to actuate a neighboring segment [5]. Another stiffness modification technique that has been proposed for soft robots is granular or layer jamming [6], [7]. Recently, an approach to change stiffness using thin sheets of a shape memory polymer was developed to change the bending stiffness of a single-DOF pneumatic robot [8]. Some of the aforementioned stiffening techniques for continuum robots enable directional stiffness control. However, in most cases, soft robot stiffening mechanisms, such as vacuum jamming approaches, typically stiffen all bending directions at once, cannot selectively change bending in one direction, or modify torsional stiffness parameters.

In this paper, we propose the integration of geometrically patterned low melting point alloys (LMPA) to enable directional stiffening in elastomeric tendon-driven continuum robots (TDCRs), generalizing prior work that has used LMPAs to stiffen soft robots (see e.g. [9]–[11]). These

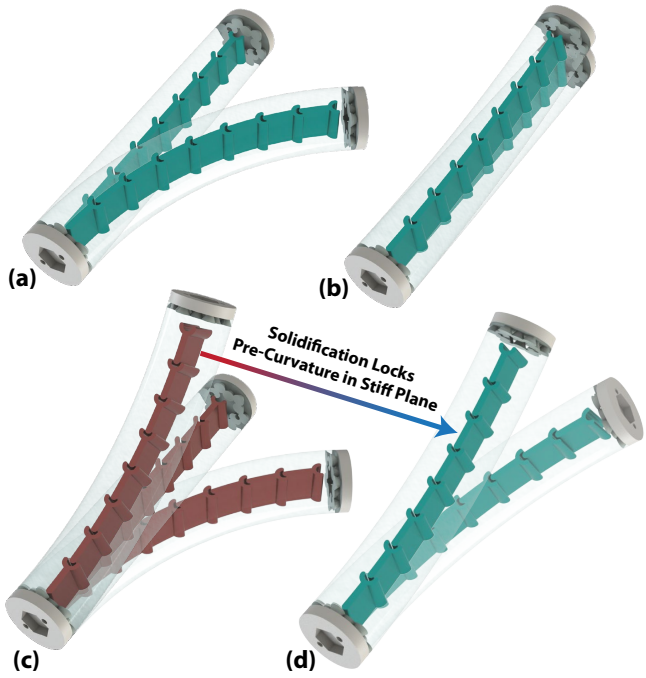


Fig. 1. Phase-changing metallic spines can change the directional bending stiffness parameters of a soft robot via melting and solidifying the spine, which is encased in a silicone matrix. A soft arm with a rectangular LMPA backbone consisting of aligned interlocking joints has a much higher bending stiffness in one plane of bending (a) than the other (b) when the spine is solidified. When the LMPA spine is liquified, the LMPA pockets become deformable, and the robot can bend in the plane in which it previously had higher stiffness (c). If the LMPA is solidified in a curved configuration, the vertebrae take on a new shape which induces a pre-curvature in the arm in the solid state (d).

This material is based upon work supported in part by the National Science Foundation (NSF) under grant number 2133027, and in part by the Natural Sciences and Engineering Research Council of Canada (NSERC) under Grant 521537544. Any opinions, findings, and conclusions or recommendations expressed in this material are those of the authors and do not necessarily reflect the views of the NSF or NSERC.

[1]Daniel S. Esser, Emily McCabe, Tayfun Efe Ertop, and Robert J. Webster III are with the Department of Mechanical Engineering, Vanderbilt University, Nashville, TN, 37203. (email: Daniel.S.Esser, Robert.Webster@vanderbilt.edu)

[2]Alan Kuntz is with the Robotics Center and the Kahlert School of Computing at the University of Utah, Salt Lake City, UT 84112, USA.

metal alloys melt at temperatures typically between room temperature and that of boiling water. They provide a way to change soft robot stiffness by an order of magnitude during use. LMPAs have been used for this purpose in a two-link continuum arm with a liquid metal core [9], a truss-like continuum arm [10], and an electrically actuated gripper [11]. These designs exhibit large LMPA cores and are designed to be flexible (similar to a traditional soft robot) when the metal is liquid, and as stiff as possible when the metal is solid (i.e. they are intended to behave as rigid links in this state). In this paper, we generalize this idea in two important ways. First, we propose to change the geometry of the LMPA within the robot from a solid core to a spine made from multiple interlocking individual LMPA chambers. The interaction between the rigid LMPA elements and the surrounding soft material enables the robot to change its curvature in the stiff state, rather than acting purely as a rigid link. Second, we propose several geometric arrangements of these spines that enable us to program desired stiffness asymmetries (i.e. independently control stiffness parameters that are typically coupled in past designs) to change the robot's behavior. This is shown conceptually for one such design in Fig. I, which has a spine that restricts bending to one plane while solid, but allows bending in all directions while liquid. In the final section, we demonstrate how a multi-segment soft robot can be directionally stiffened via selective melting and solidification of the LMPA spines.

Our proposed design enables control of specific stiffness parameters using interlocking individual LMPA chambers that form a spine, and can be heated with heating wire to switch between soft (liquid) and stiff (solid) states. This concept was loosely inspired by two biological features. Biological spines consist of vertebrae that interlock and exhibit stiffness and range of motion variations in different directions. For example, snakes exhibit preferential bending in the plane across which they locomote [12], and the human spine also has differing ranges of motion and stiffness in different directions of bending [13]. The other biological feature that our designs draw inspiration from are the nonlinear muscle fibers present in biological tentacles and trunks [14], [15] which have inspired tendon-driven continuum robots for a wide variety of applications [16]–[20]. We use nonlinear tendons to apply more general loads than linear routing paths, including coupled, non-planar forces and moments. The effects of nonlinear tendons have been modeled in the past [21], and can be used to shape workspaces to task objectives [22], [23]. It is worth noting that with tendon routing alone, design choices must be made a priori. But by combining curved routing with LMPA spines, we have the potential for new effects. For example, we demonstrate how to turn on and off the certain bending modes, thus changing how actuating each tendon moves the soft robot.

To illustrate the ability of LMPA spines to enable a robot to switch between two different stiffness states by liquifying or solidifying the spine, we built four example prototypes. The first (referred to as "Prototype 1" in Section III) has a spine of interlocking elements aligned in the same plane, enabling it to exhibit higher stiffness in one bending plane than the other. The second (Prototype 2) has stacked semi-circular disks that shift the stiffness center away from the central axis of the device. This makes it able to bend to higher curvatures in one in-plane direction than the other. The third (Prototype 3 described in Section IV) has a hinged LMPA spine similar to Prototype 1, except each successive hinge is rotated 90 degrees with respect to its neighbors, resulting in a high torsional stiffness about the central axis of the device, while still enabling bending in both directions, even when the spine is in the solid state. The last prototype (Prototype 4, which we demonstrate in Section VI) has a continuous cylindrical chamber-filled LMPA, as has been previously suggested in the literature [9]. Before describing each prototype in detail and experiments using it (Sections III and IV), we first describe how each was fabricated in Section II.

## II. Fabricating Soft Robots with LMPA Spines

To construct each prototype, we first cast each component of the LMPA backbone. We then co-molded silicone with the LMPA and a heating wire, with each vertebra in the multi-section spines residing in its own closed chamber within the surrounding silicone. Fig. 2 shows the fabrication process for Prototype 3. The process is similar for all the other prototypes with the only difference being the backbone geometry.

We use Fields metal, which has a melting temperature of $62^\circ$ C, as the LMPA in our prototypes. Fabrication begins by creating a 3D-printed (*Formlabs Grey Pro*) positive mold of the LMPA vertebra/backbone shapes (see Fig. 2.a). We then cast silicone in the 3D-printed mold to create a flexible, heat-resistant negative mold for the LMPA vertebra. LMPA is then melted and cast into the silicone mold. Once solid, the vertebrae can be removed as shown in Fig. 2.b. In the case of Prototype 3 only, two sections of each LMPA vertebra were cast separately and then joined together with a soldering iron (Fig. 2.c). Next, we placed the LMPA segments on an alignment jig to define their arrangement and attached them to one another to form a chain using a silicone adhesive (*Smooth On*) as shown in Fig. 2.c. This silicone adhesive separates each vertebra from the others (they interlock with a thin layer of silicone adhesive between them) so that each resides in its own distinct chamber within the overall soft robot. Thus, they can be cycled from solid to liquid and back as many times as desired without the LMPA flowing from one vertebra into another.

After the spine is constructed in this way, we mold the cylindrical elastomer around it. We first place the spine in the center of a cylindrical mold, with the alignment jig constraining its position. After the first silicone molding step, the alignment jig is removed from the partially molded prototype, as shown in Fig. 2.d. Before casting the silicone for the final time, we placed a heating wire made out of 28 Gauge nichrome wire encased in a polyimide sheath to electrically (but not thermally) insulate it from the metal.

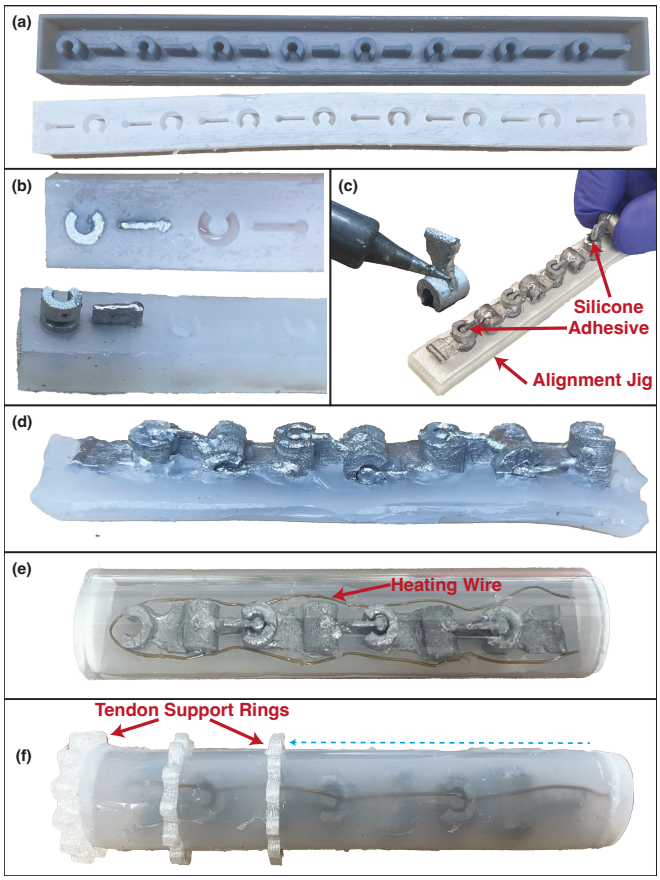


Fig. 2. Fabrication process. (a) We 3D printed a positive of the LMPA vertebra shapes to create a silicone mold. (b) Silicone mold from (a) is filled with the LMPA to create constituent elements of the spine. (c) We rigidly attach these components by melting them with a soldering iron to form individual vertebrae. Subsequently, they are assembled together into the spine on the alignment jig using silicone adhesive at the joints. (d) To constrain the location of the spine, we first cast the spine with the alignment jig in the cylindrical mold and then remove the alignment jig, leaving the spine partially embedded. (e) The second molding step fills the rest of the mold with silicone, covering the spine and heating wire in position in the prototype. (f) After the final molding step, we slide the TPU tendon support rings on and affix them using a small amount of silicone adhesive.

Next, we insert the assembly back into the cylindrical mold and fill the remaining volume with silicone. We use 00-30 Durometer silicone (*Ecoflex 30, Smooth On*) in all prototypes in this paper. 3D-printed caps are co-molded into the proximal and distal ends of the prototype, and they have a threaded hole that enables two distinct sections to be attached in series to form a multi-section modular manipulator, as demonstrated in Section VI. Finally, we slide rings with eyelets for tendon routing around the prototype. These are printed with 95 durometer TPU (*Bambu Carbon X1 printer*). The tendon rings were undersized by 0.5mm and friction fit around the manipulator, and the ring closest to the robot's tip was glued to the tip using the same silicone adhesive used to encase the vertebra.

We heat the prototypes by connecting the nichrome wire to a DC power supply; the prototypes with a spine (prototypes 1-3) can be melted from room temperature in approximately 50s with 2A ($\approx$ 15V). They take approximately 90 seconds to cool from room the melted state to the solid state.

## III. LMPA Spines to Modify In-Plane Bending

In this section, we discuss Prototypes 1 and 2, in which spines are used to modify the in-plane bending characteristics (both stiffness and range of motion) of a soft robot. We designed two different LMPA spines with the purpose of introducing a difference of stiffness between two orthogonal planes of bending, and shifting the center of stiffness within the cross-section, respectively.

To achieve this, Prototype 1 consists of an LMPA spine with rectangularly shaped vertebrae. The rectangular cross-section of the spine is much narrower in one direction than the other, resulting in a higher stiffness in that direction. The vertebrae mechanically interlock with a pin-joint-like interface, so that they do not slip in shear relative to each other but still allow bending in the compliant direction. The second prototype has a spine consisting of stacked semi-circular LMPA disks. The semi-circular spine is embedded in the cross-section such that its flat edge is on the centerline of the cylindrical elastomer body of the robot. The offset centroid of the spine from the central axis of the robot creates a preferential bending direction.

In the subsections that follow, we first give a brief overview of bending stiffness for rods with stiffness variation across their cross sections, and then use these equations as a means to experimentally infer stiffness from curvature and tendon tension, given the constant curvature assumption [24].

### A. From Stiffness Parameters to Bending Profiles

To characterize the bending stiffness prototypes, we routed straight tendons that are offset in the direction of the principal axes (for Prototype 1) and on either side of the stiffness center along the major axis (for Prototype 2) to evaluate their respective stiffness properties. We use the constant curvature assumption for stiffness characterization, though we envision more complex models being used in the future for robot control (e.g. [21]).

An applied tip moment $M$ will cause the prototype to bend into an arc with curvature $\kappa = C_b M$, where the bending compliance $C_b = \frac{1}{K_b}$ is the inverse of the stiffness $K_b$. The bending stiffness is based on the Young's modulus distribution across the cross-section, and may be different in each direction:

$$K_{b,y} = \int_A E(x,y)x^2 dA, \tag{1}$$

where $K_{b,y}$ is the bending stiffness about the $y$ axis of the cross-section, and $E(x,y)$ is the modulus of elasticity. For an arbitrary cross-section, the stiffness center (also called the normal force center) is the point in the cross-section with no strain when the member experiences pure bending. The position of the stiffness center is:

$$x_{sc} = \frac{\int_A Ex dA}{\int_A E dA} \tag{2}$$

and similarly for the $y$ coordinate.

A force applied further from the stiffness center will create a larger moment than a force applied closer, and

will thus result in higher curvature. Similarly, the robot can have different stiffness in different planes based on spine geometry. The LMPA spine (which has rectangular cross sections) in Prototype 1 gives it a significantly higher stiffness in one direction than the other, and the spine in Prototype 2 (which is offset from the center of the device) causes higher curvature in one in-plane bending direction than the other.

To verify these expected behaviors experimentally, we measure the curvature of an actuated prototype (described in the last paragraph of this subsection) by applying known loads on each tendon, all with the same radial offset from the geometric center. Prototype 1 has rectangular LMPA vertebrae aligned with the x-axis, and the two tendons apply known tension to the prototype. Prototype 2 has LMPA vertebrae offset in the $-\hat{x}$ direction and tendons on opposite sides of the prototype.

For Prototype 1, $C_{b,x}$ and $C_{b,y}$ are the slopes of the curvature-moment plot for tendons offset in the x and y planes. For Prototype 2 with an offset stiffness center, $C_{b+}$ and $C_{b-}$ are the slopes of the moment-curvature plot for the tendons in the $+\hat{x}$ and $-\hat{x}$ offset from the center. For future modeling, we would like to express the stiffness parameters in terms of the position of the stiffness center (in $x$ in this case) as well as the compliance at the stiffness center, which is equal for positive and negative moments. If $r_t$ is the distance of a tendon from the center, we know that $\kappa = C_{b+}F_t r_t$ and $\kappa = C_{b-}F_t r_t$, where +/- indicates the direction of bending. We would like to find the position of the stiffness center where the bending stiffness $k_b$ is the same in both directions:

$$\kappa = C_{sc}F_t(x_t - x_{sc}), \tag{3}$$

where $C_{sc}$ is the compliance in both directions (at the stiffness center), $F_t$ is the tendon tension, $x_{sc}$ is the position of the stiffness center and the position of each tendon is $x_t = \pm r_t$ depending on which side the tendon is on. Note: here we assume that the curvature is the same across the cross-section (a good assumption for thin rods). By equating the curvatures in the positive and negative direction with Eqn. 3, we can express the bending stiffness at the stiffness center and its offset as:

$$C_{sc} = \frac{1}{2}(C_{b+} + C_{b-}) \tag{4}$$

$$x_{sc} = \frac{C_{b+} - C_{b-}}{2(C_{b+} + C_{b-})} r_t. \tag{5}$$

We use these equations to convert the slope of the line of best fit in Fig. 5 to the stiffness parameters in Table II.

To measure the prototype curvature in various bending directions, we used three RGB-D cameras (*Intel RealSense D405*), as shown in the inset of Fig. 3, which were registered to the base frame of the robot using 3D-printed calibration targets. To validate the accuracy of this measurement setup, we 3D printed six tubes with a constant curvature bend with tip angles evenly spaced from 15 to 90 degrees of bending, with the same length and diameter as the silicone prototypes.

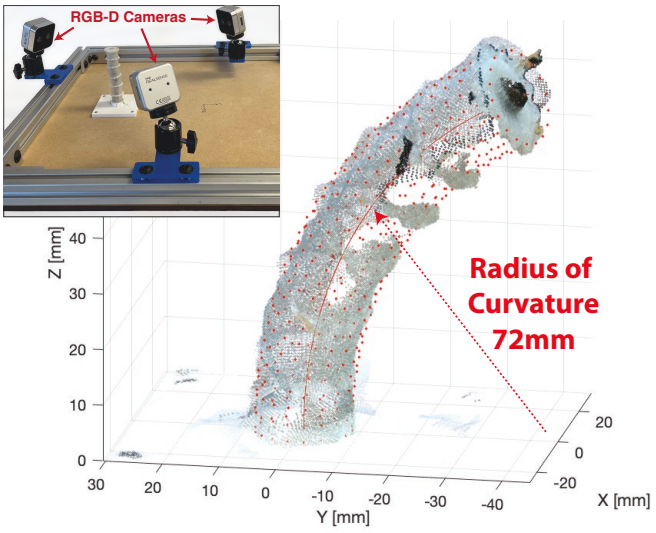


Fig. 3. Example of one bending configuration with a constant curvature model (in red) fit to a pointcloud. The RGB-D camera setup to acquire the pointclouds is shown in the inset.

The 3D camera setup was able to measure these targets with an average accuracy of $0.49°$. An example output from this camera setup is shown in Fig. 3; the constant curvature model was fit to the pointcloud data as shown in red, to measure the curvature $\kappa$. The tendons were pulled with various calibration weights to determine the relation between curvature $\kappa$ and tip moment so that we can calculate the bending parameters.

### B. Planar Bending Results

*1) Prototype 1: Bending Stiffness in Two Different Planes:* The results of the bending stiffness characterization for Prototype 1, with LMPA segments aligned with the x-axis, are shown in Fig. 4. The second moment of area of a rectangle is $I_x = \frac{l^3 w}{12}$, where $l$ is the length of the cross-section in the $\hat{x}$ direction. Therefore, we expect the prototype to be much stiffer when bending in the XZ plane than the YZ plane when the metal is solid. The slope of the light blue line in Fig. 4 represents the bending compliance in the direction aligned with the liquid metal, while the dark blue shows the stiffness in the direction perpendicular to the LMPA segments, both in the solid state. The compliance is clearly much larger in one direction than the other. The slope of the red and orange lines represent the compliance in the same two planes when the LMPA spine is melted. The overall compliance of the prototype in the liquid state is much higher and similar in both bending planes.

*2) Prototype 2: Shifted Stiffness Center:* Prototype 2 consists of stacked liquid metal semi-circular vertebrae with a radius of 5mm. In the solid state, since the stiffness of the prototype is dominated by that of the LMPA spine, we expect that the stiffness center will be shifted close to the centroid of the semicircle. The centroid of a semicircle is given by $\bar{x} = \frac{4r}{3\pi}$; for $r = 5$mm, the centroid of the spine is 2.1mm, which is close to the measured stiffness center offset

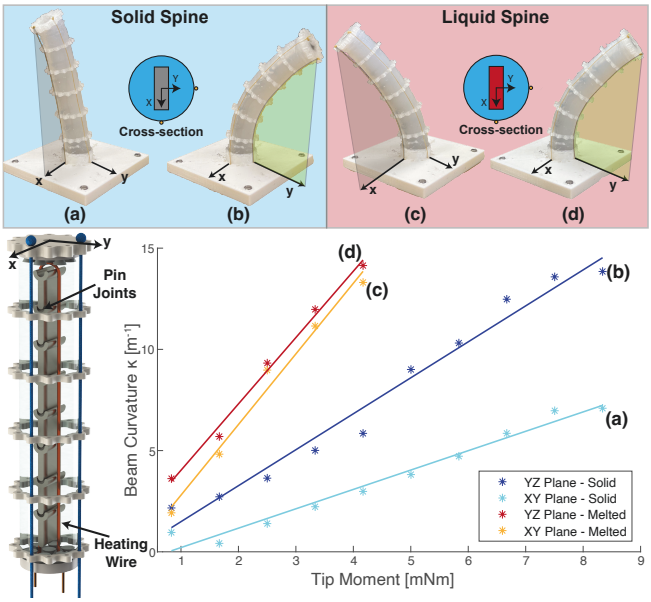


Fig. 4. In the solid state, prototype 1 has a significantly higher stiffness in the major axis (x) than minor axis (y). For the same tendon tension, it exhibits less bending in the plane aligned with the LMPA spine (a) as compared to the other direction (b). In the liquid state, the directional bending stiffness are similar (see (c) and (d)), and the prototype behaves more similarly to a conventional soft robot with a symmetric stiffness profile.

| Prototype 1 | | | | |
|---|---|---|---|---|
| | Bending (LMPA Plane) | | Bending (Orthogonal to LMPA) | |
| | Stiffness $K[\mathrm{Nm/m^{-1}}]$ | Compliance $C[\mathrm{m^{-1}/Nm}]$ | Stiffness $K[\mathrm{Nm/m^{-1}}]$ | Compliance $C[\mathrm{m^{-1}/Nm}]$ |
| Solid | 1.03 | 0.972 | 0.541 | 1.85 |
| Liquid | 0.286 | 3.50 | 0.303 | 3.30 |

TABLE I

BENDING STIFFNESS PARAMETERS FOR PROTOTYPE 1

of 1.70 mm in the negative $\hat{x}$ direction. The stiffness center is the Young's modulus-weighted centroid of the cross-section, therefore we expect it to be between the geometric center of the rod (where it would be for a homogeneous elastomer) and the centroid of the spine (where it would be without the elastomer), but closer to the spine because of the large difference in stiffness.

As a result of the offset stiffness center in the solid state, the prototype exhibits more bending in the positive direction than the negative direction for two tendons opposite each other and equally spaced from the geometric center. In the liquid state, the stiffness center is close to the geometric center, and the bending stiffness is similar in both directions within the plane, matching our expectations.

| Prototype 2 | | | |
|---|---|---|---|
| | S.C. Offset [mm $\hat{x}$] | Bending Compliance $C[\mathrm{m^{-1}/Nm}]$ | Bending Stiffness $K[\mathrm{Nm/m^{-1}}]$ |
| Solid | $-1.70$ | 0.919 | 1.09 |
| Liquid | $-0.05$ | 4.27 | 0.234 |

TABLE II

BENDING STIFFNESS PARAMETERS FOR PROTOTYPE 2

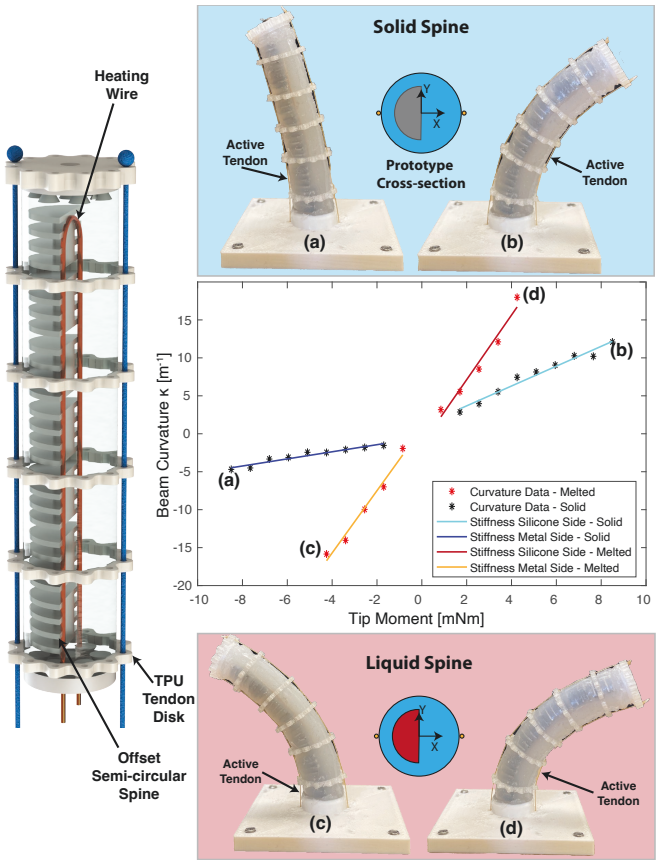


Fig. 5. Prototype 2 has its stiffness center offset in the negative direction in the solid state, thus exhibiting more bending in the positive direction than the negative direction, for two tendons opposite each other. In the liquid state, the stiffness center is close to the geometric center, and the bending stiffness is similar in both directions in the plane.

## IV. LMPA SPINE TO CHANGE TORSIONAL STIFFNESS

In the prior section, we explore how vertebral geometry can change the bending stiffness of a prototype. Continuum robots frequently experience torsion, either from non-linearly routed tendons [21], torques/moments from magnetic actuators [25], or external loads. Therefore, changing torsional stiffness during use is another way to modify a soft robot's behavior.

Prototype 3, shown in Fig. 7.a, has liquid metal segments shaped in a pin joint arrangement that alternates in the $x$ and $y$ directions over arclength. This enables bending in both directions while the joints are solid, but restricts torsion about the local $z$ direction. Once melted, the liquid metal segments are compliant and no longer resist torsion.

To measure the torsional stiffness of Prototype 3 (shown in Fig. 7.a), we apply a torsional moment at the tip of the prototype and measure the rotation of the tip. The test setup shown in Fig. 7.b constrains the base of the segment, and a length of string is tied and wrapped around the tip of the robot to apply torque. The pulley directs the string at a fixed offset tangent to the top of the prototype. Calibration weights apply known loads to the string. The screw attached to the tip of the robot fits loosely through the hole in the stand, and

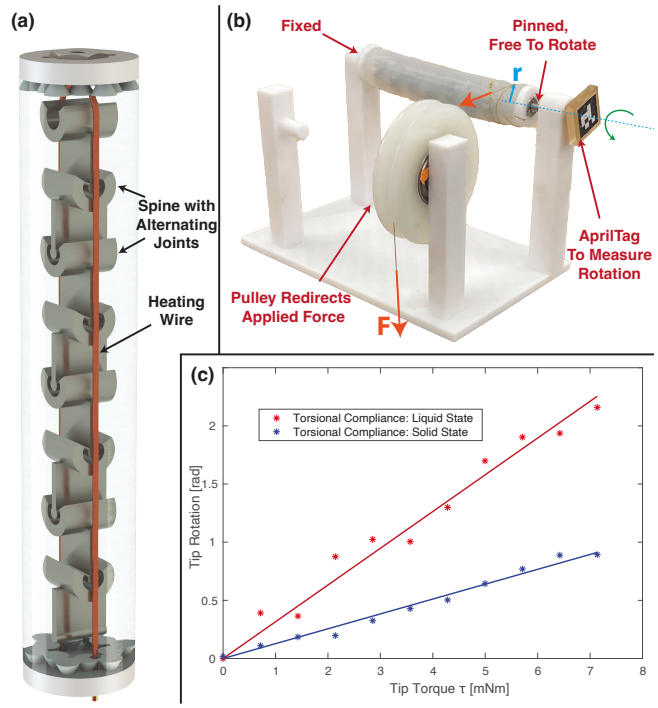


Fig. 7. We measured the torsional stiffness of Prototype 3 (shown in (a)) with the measurement setup shown in (b), which constrains one end of the prototype and twists the prototype about its axis with a string; the rotation at one end is measured with an AprilTag. (c) Tip rotation as a function of applied torque shows that the torsional compliance is much greater in the liquid state than solid state.

the other end of the screw has an optical tracking marker affixed to it. We use a camera to track the rotation of the tip frame as the prototype twists.

In this characterization, we consider Prototype 3 as a torsional spring, with variable stiffness, dependent on the state of the spine. Figure 7.c clearly shows a large difference in the tip rotation when the spine is melted, and the change in stiffness/compliance is presented in Table III.

| Prototype 3 | | |
|---|---|---|
| | Torsional Compliance $C_t$[rad/mNm] | Torsional Stiffness $K_t$[mNm/rad] |
| Solid | 0.128 | 7.82 |
| Liquid | 0.316 | 3.17 |

TABLE III
TORSIONAL STIFFNESS PARAMETERS FOR PROTOTYPE 3

## V. COMBINING SPINES AND CURVED TENDONS

In Sections III and IV, we characterize the three prototypes with LMPA spines in planar bending and pure twisting. In this section, we explore how the combination of tendon routing and changing stiffness properties can achieve a diverse set of soft robot shapes with a small number of actuated degrees of freedom. Helical tendons also apply both bending and torsional deformations to continuum robots, as the tendon tries to unwrap itself when tensioned. This twisting effect can be beneficial to axially rotate the end effector. Helical tendons can also be used to move the end effector while holding its orientation constant, which can be used for e.g. pick-and-place tasks as described in [21]. We first show how the deformations caused by nonlinear tendons can be reconfigured by changing the bending and torsional stiffness parameters (i.e. solidifying and liquefying the spine). Using Prototype 1, we routed a helical tendon that crosses over the major (stiff) axis: the tendon angle over arclength $\phi(s) = \frac{\pi s}{L} - \frac{\pi}{2}$, as shown in Fig. 6.a.I. When the backbone is in the liquid state and the compliance is similar in both directions (see Fig. 4), the backbone deforms in a non-planar, roughly helical shape (Fig. 6.a.III). However, when the backbone is solid, the helical tendon deforms the prototype in a roughly planar s-bend, because tendon forces in the $\hat{x}$ direction result in minimal strain (Fig. 6.a.II).

Next, we explore axial rotation of the robot's tip. Prototype 3, which changes torsional stiffness as the spine solidifies and liquefies, can restrict or enable twisting while allowing bending in all directions. To demonstrate this, we routed

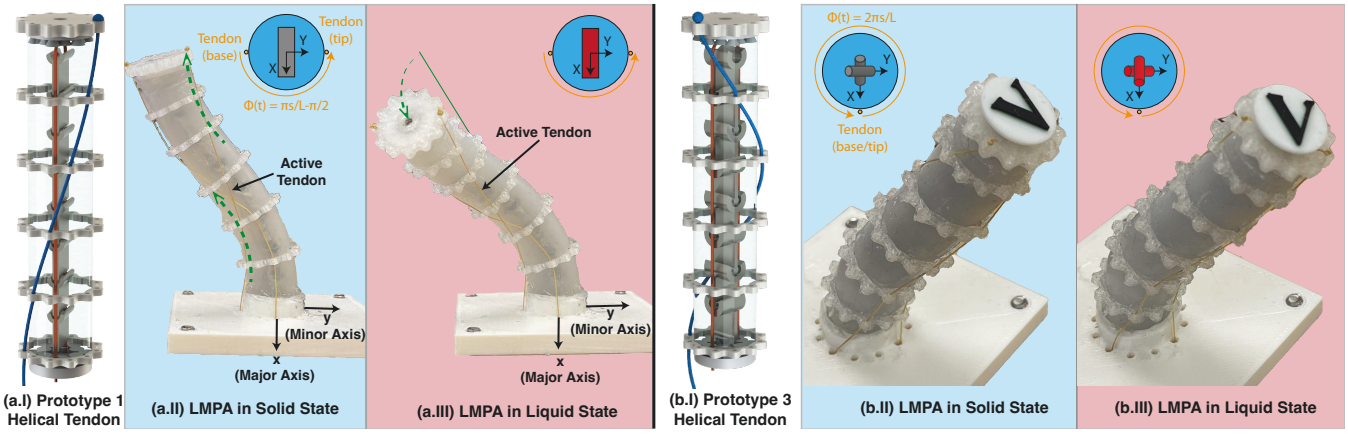


Fig. 6. Helical tendons apply forces and moments in multiple directions. (a.I) With a helical tendon, the spine in Prototype 1 restricts the deformation to its compliant plane in the solid state (a.II), and the arm bends into an s-shaped configuration even though the tendon applies loads out of this plane. In the liquid state (a.III), the stiffness is similar in both planes, and the robot bends into a non-planar shape. With a helical tendon on Prototype 3 (b.I), the arm bends in a non-planar shape (b.II). When melted, the bending profile is similar but with more twist because the spine no longer restricts torsion (b.III).

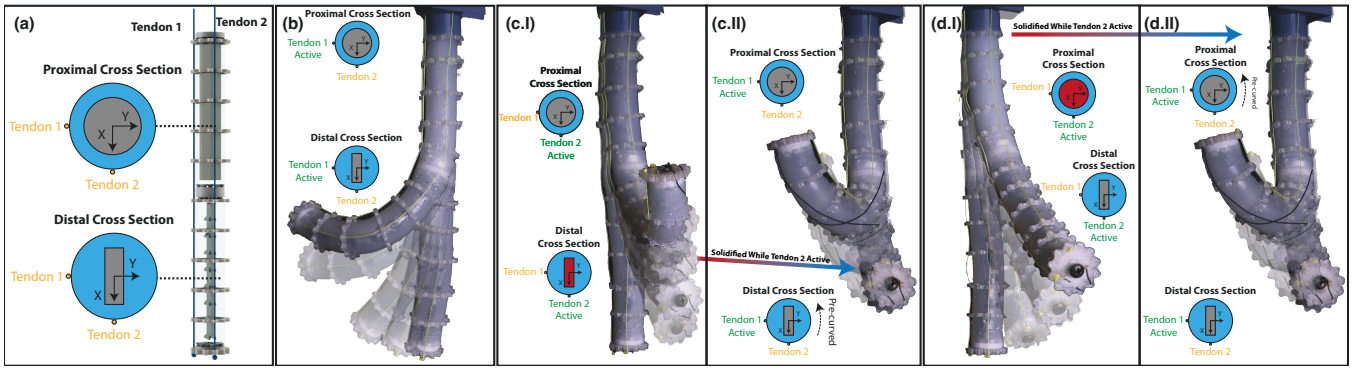


Fig. 8. By chaining segments with different spines, a wide range of shapes can be achieved using only two straight-routed tendons. (a) The modular manipulator consists of Prototype 4 connected to Prototype 1. (b) When both segments are solid, tendon 1 only bends the distal section. (c.I) When the distal section is melted it can be actuated in the XZ plane while the proximal section is solid. (c.II) By solidifying segment 2 in a curved state, this induces a pre-curvature in the distal segment, changing how tendon 1 deforms this section. (d.I) Melting the proximal segment allows it to be actuated. (d.II) Segment 1 is solidified with a curved shape, changing the pose of the start of segment 2, and the direction tendon 1 actuates it in.

Prototype 3 with a helical tendon that wraps around itself with $\phi(s) = \frac{2\pi s}{L}$ (Fig. 6.b.I). In Fig. 6.b.II and 6.b.III, the prototype deforms in a similar helical shape but with less twisting in the solid than liquid state.

## VI. Connecting Segments to form a Soft Arm

In the prior sections, we demonstrate how spinal geometries result in specific stiffness capabilities that depend on the state of the metallic elements, and how curved or straight tendon routings can deform these segments into different shapes when vertebrae are in the solid or liquid states. By chaining these segments together, with continuous tendons running the length of the soft arm, we can use both tendons and metal state changes to achieve a larger range of space curve shapes than would be possible with either alone. By changing liquid metal states in different sections of the robot, we can change the bending stiffness parameters within a section, or induce a pre-curvature by melting a segment, actuating it, and then solidifying the spine in a curved state. We henceforth refer to a configuration as a particular liquid metal state in each segment, as well as the potential precurvature of the LMPA backbone segment(s) that are solid.

As a demonstration of this, we connect Prototype 4 to Prototype 1 with straight tendons routed in orthogonal planes. With different stiffness properties between segments, we can actuate the distal section in its compliant direction with a tendon that runs the entire length (Fig. 8.b). By melting, actuating, and re-solidifying an LMPA spine in a curved configuration (Fig. 8.c.I), we can precurve the LMPA spine, changing how that spine deforms once it is solidified in a curved configuration (Fig. 8.c.II). In this configuration, the prototype has different bending parameters. By melting the proximal section, we can selectively bend it in the XZ plane while keeping the distal segment straight because it is stiffer in this plane (Fig. 8.d.I). Inducing a curvature in the distal segment and re-solidifying it changes the pose of the start of the second segment and the direction that it bends under an actuation input (Fig. 8.d.II). The multitude of configurations possible with just two tendons is clearly greater than a homogeneous soft robot with the same two straight tendons, which would only be able to deform in a constant-curvature shape in two directions.

## VII. Discussion

The LMPA backbones developed in this work enable control over various parameters of the stiffness properties of soft robots. Rather than re-routing the tendons, we can reconfigure how the tendons deform the prototype by changing asymmetric stiffness properties, resulting in a new workspace with the same tendon configuration. This is particularly useful when actuation inputs apply coupled loads, for example, a helical tendon that applies torque and moments in different directions along the length of the prototype. By restricting some of these deformations with stiffness control, the robot can achieve a different shape. We also foresee stiffness control in this manner applying to other classes of robots that are actuated via coupled, multi-directional forces and moments. For example, magnetic soft robots, actuated by a homogeneous field or gradient, could be controlled to bend or twist in specific ways in different segments of the arclength using stiffness control, even if the force and moment at every point in the soft robot cannot be arbitrarily specified by the applied field. Directional stiffness control can also aid in resisting external loads; for example, increasing bending stiffness in one direction could resist gravitational loading, while changing the torsional stiffness could be used to rotate or twist an object. In the future, we envision various designs of robots that can toggle the effect of spinal morphology on overall stiffness on and off during operation to adapt itself to changing task requirements.

Our preliminary characterization of these LMPA spine-based soft robots demonstrates that these composite structures can be modeled as having linear bending and torsional stiffness and that the LMPA phase changes can be modeled as a change in these stiffness parameters. This indicates that such robots, despite their unique mechanical design, could be modeled using similar methods to more conventional

TDCRs, for example in [21], if the full bending stiffness matrix is calibrated for each segment in each metal state.

We show the proof-of-concept feasibility of chaining these LMPA spines sequentially with independent control over their deformation properties. In this work, we changed the state of an entire prototype segment with a continuous backbone. However, since the individual vertebrae are self-contained, it would be feasible to independently melt shorter segments of the spine to obtain more localized control, e.g. to enable a short section of the spine to bend sharply around a curve in a particular direction. Our LMPA spines are controlled with a small embedded heating wire and an external electrical source. With other actuated stiffening mechanisms (i.e. tendon, backbone, pneumatic, or vacuum), the amount of stiffness degrees of freedom is governed by the number of actuators or fluid paths. We hypothesize that we can achieve higher fidelity control using LMPA spines, as they can be locally heated by many independently controlled heating wires, which are a fraction of a millimeter in diameter.

## VIII. CONCLUSIONS

Soft robots with geometrically-patterned LMPA elements embedded in a silicone matrix can be designed with directional stiffness properties. The stiffness properties can be toggled via the application of heat, and sequential state changes and actuation can change the pre-curvature. In future, these LMPA-tendon modules can be designed to create task-specific manipulators. As opposed to using many tendons to create complex shapes, which increases the complexity and potentially the size of the manipulator, LMPA segments can change their state with very thin electrical heating wires. There is even the potential to selectively melt and solidify individual vertebrae along the arclength, for finer control of the soft robot's stiffness in various directions. This type of stiffness modification offers an exciting opportunity for robots to be both compliantly safe and stiff enough, in the right directions, to apply the forces required in various applications.

## REFERENCES


[1] G. Del Giudice, Long Wang, Jin-Hui Shen, K. Joos, and N. Simaan, "Continuum Robots for Multi-Scale Motion: Micro-Scale Motion through Equilibrium Modulation," in *2017 IEEE/RSJ International Conference on Intelligent Robots and Systems (IROS)*. IEEE, 2017, pp. 2537–2542.

[2] J. Barrientos-Diez, M. Russo, X. Dong, D. Axinte, and J. Kell, "Asymmetric Continuum Robots," *IEEE robotics and automation letters*, vol. 8, no. 3, pp. 1279–1286, 2023.

[3] K. Oliver-Butler, J. Till, and C. Rucker, "Continuum Robot Stiffness under External Loads and Prescribed Tendon Displacements," *IEEE Transactions on Robotics*, vol. 35, no. 2, 2019.

[4] A. Shiva, A. Stilli, Yohan Noh, A. Faragasso, I. De Falco, G. Gerboni, M. Cianchetti, A. Menciassi, K. Althoefer, and H. A. Wurdemann, "Tendon-Based Stiffening for a Pneumatically Actuated Soft Manipulator," *IEEE robotics and automation letters*, vol. 1, no. 2, pp. 632–637, 2016.

[5] C. Pogue, P. Rao, Q. Peyron, J. Kim, J. Burgner-Kahrs, and E. Diller, "Multiple Curvatures in a Tendon-Driven Continuum Robot Using a Novel Magnetic Locking Mechanism," in *IEEE International Conference on Intelligent Robots and Systems*, vol. 2022-October. Institute of Electrical and Electronics Engineers Inc., 2022, pp. 472–479.

[6] B. Yang, R. Baines, D. Shah, S. Patiballa, E. Thomas, M. Venkadesan, and R. Kramer-Bottiglio, "Reprogrammable Soft Actuation and Shape-Shifting via Tensile Jamming," *Sci. Adv*, vol. 7, 2021.

[7] Y. Li, Y. Chen, Y. Yang, and Y. Wei, "Passive Particle Jamming and Its Stiffening of Soft Robotic Grippers," *IEEE transactions on robotics*, vol. 33, no. 2, pp. 446–455, 2017.

[8] J. Santoso, E. H. Skorina, M. Salerno, S. de Rivaz, J. Paik, and C. D. Onal, "Single Chamber Multiple Degree-of-Freedom Soft Pneumatic Actuator Enabled by Adjustable Stiffness Layers," *Smart materials and structures*, vol. 28, no. 3, p. 35012, 2019.

[9] F. Alambeigi, R. Seifabadi, and M. Armand, "A Continuum Manipulator with Phase Changing Alloy," in *2016 IEEE International Conference on Robotics and Automation (ICRA)*, 2016, pp. 758–764.

[10] J. Zhang, B. Wang, H. Chen, J. Bai, Z. Wu, J. Liu, H. Peng, and J. Wu, "Bioinspired Continuum Robots with Programmable Stiffness by Harnessing Phase Change Materials," *Advanced Materials Technologies*, vol. 8, no. 6, 3 2023.

[11] J. Shintake, B. Schubert, S. Rosset, H. Shea, and D. Floreano, "Variable Stiffness Actuator for Soft Robotics using Dielectric Elastomer and Low-Melting-Point Alloy," in *2015 IEEE/RSJ International Conference on Intelligent Robots and Systems (IROS)*. IEEE, 2015, pp. 1097–1102.

[12] D. J. Jurestovsky, B. C. Jayne, and H. C. Astley, "Experimental Modification of Morphology Reveals the Effects of the Zygosphene-Zygantrum Joint on the Range of Motion of Snake Vertebrae," *Journal of Experimental Biology*, vol. 223, no. 7, 4 2020.

[13] D. A. Neumann, *Kinesiology of the Musculoskeletal System: Foundations for Rehabilitation*, 3rd ed., 2016.

[14] A. K. Schulz, J. S. Reidenberg, J. Ning Wu, C. Ying Tang, B. Seleb, J. Mancebo, N. Elgart, and D. L. Hu, "Elephant Trunks Use an Adaptable Prehensile Grip," *Bioinspiration & biomimetics*, vol. 18, no. 2, p. 26008, 2023.

[15] Y. Yekutieli, R. Sagiv-Zohar, R. Aharonov, Y. Engel, B. Hochner, and T. Flash, "Dynamic Model of the Octopus Arm. I. Biomechanics of the Octopus Reaching Movement," *Journal of Neurophysiology*, vol. 94, no. 2, pp. 1443–1458, 2005.

[16] J. Burgner-Kahrs, D. C. Rucker, and H. Choset, "Continuum Robots for Medical Applications: A Survey," *IEEE transactions on robotics*, vol. 31, no. 6, pp. 1261–1280, 2015.

[17] D. R. Mangels, J. Giri, J. Hirshfeld, and R. L. Wilensky, "Robotic-Assisted Percutaneous Coronary Intervention," *Catheterization and cardiovascular interventions*, vol. 90, no. 6, pp. 948–955, 2017.

[18] F. Campisano, A. A. Remirez, C. A. Landewee, S. Calo, K. L. Obstein, R. J. Webster III, and P. Valdastri, "Teleoperation and Contact Detection of a Waterjet-Actuated Soft Continuum Manipulator for Low-Cost Gastroscopy," *IEEE robotics and automation letters*, vol. 5, no. 4, pp. 6427–6434, 2020.

[19] S. Jiang, J. Lou, Z. Yang, J. Dai, and Y. Yu, "Design, Analysis and Control of a Novel Tendon-Driven Magnetic Resonance–Guided Robotic System for Minimally Invasive Breast Surgery," *Proceedings of the Institution of Mechanical Engineers. Part H, Journal of engineering in medicine*, vol. 229, no. 9, pp. 652–669, 2015.

[20] Z. Yang, B. Zhao, L. Bo, X. Zhu, and K. Xu, "CurviPicker: a Continuum Robot for Pick-and-Place Tasks," *Assembly automation*, vol. 39, no. 3, pp. 410–421, 2019.

[21] D. C. Rucker and R. J. Webster III, "Statics and Dynamics of Continuum Robots with General Tendon Routing and External Loading," *IEEE Transactions on Robotics*, vol. 27, no. 6, 2011.

[22] M. Rox, A. Copinga, R. Naftel, I. R. Webster, and A. Kuntz, "Optimizing Continuum Robot Tendon Routing for Minimally Invasive Brain Surgery," in *Hamlyn Symposium on Medical Robotics*, London, UK, 2022.

[23] J. Starke, E. Amanov, M. T. Chikhaoui, and J. Burgner-Kahrs, "On the Merits of Helical Tendon Routing in Continuum Robots," in *2017 IEEE/RSJ International Conference on Intelligent Robots and Systems (IROS)*. IEEE, 2017, pp. 6470–6476.

[24] R. J. Webster and B. A. Jones, "Design and Kinematic Modeling of Constant Curvature Continuum Robots: A Review," *The International Journal of Robotics Research*, vol. 29, no. 13, pp. 1661–1683, 2010.

[25] D. Chathuranga, P. Lloyd, J. H. Chandler, R. A. Harris, and P. Valdastri, "Assisted Magnetic Soft Continuum Robot Navigation via Rotating Magnetic Fields," *IEEE robotics and automation letters*, vol. 9, no. 1, pp. 1–8, 2024.